Dalton Transactions

ROYAL SOCIETY OF CHEMISTRY

PAPER

View Article Online
View Journal | View Issue

Cite this: *Dalton Trans.*, 2025, **54**, 694

Simple and easy functionalization of *para*-hydroxy POCOP-M (M = Ni(II), Pd(II)) pincer complexes: synthesis of multimetallic species†

Juan S. Serrano-García, [a] Marco Antonio García-Eleno, *[b] Antonino Arenaza-Corona, [a] Ernesto Rufino-Felipe, [a] Hugo Valdés, [c] Simon Hernandez-Ortega [a] and David Morales-Morales *[a]

A facile and efficient method for synthesizing mono- and bi-metallic pincer complexes (**3-Ni/Ni** and **3-Ni/Pd**) has been developed. The procedure involves a 1 : 1 stoichiometric reaction of a *para*-hydroxy POCOP pincer complex with cyanuric chloride in the presence of $[NaB(OMe)_4]$, which selectively affords the mono-substituted pincer complexes (**2-Ni** and **2-Pd**). These complexes are then further reacted with another equivalent of the *para*-hydroxy POCOP pincer complex to produce the desired multimetallic species (**3-Ni/Ni** and **3-Ni/Pd**). The complexes can be easily isolated in moderate to good yields using chromatographic column purification. This straightforward synthesis procedure offers an attractive option for the preparation of multimetallic complexes. Furthermore, the molecular structures of complexes **2-Ni**, **2-Pd**, **3-Ni/Pd** and **3-Ni/S** were determined. The crystal packing of the structures was stabilized by various interactions including C–H···X (X = N, Cl, and F), π···π, and C–F···F interactions, contributing to their unique topologies. While **2-Ni** and **2-Pd** complexes exhibit similar molecular structures, they display distinct arrangements in their crystalline packing, such as monomeric chains in 1D arrangement along the *c*-axis for **2-Ni**, and a symmetric dimeric species creating a 2D arrangement in the direction of the *bc*-axes for **2-Pd**. The latter was corroborated by Hirshfeld surface analysis and 2D dimensional fingerprint plots of each crystal structure.

Received 10th October 2024,
Accepted 13th November 2024

DOI: 10.1039/d4dt02841d

rsc.li/dalton

Introduction

Pincer complexes serve as excellent platforms for synthesizing highly active catalysts and advanced materials. They have the ability to catalyze several reactions that are vital in many chemical industries, including (de)hydrogenation and cross-coupling, among others, making them essential for many applications.[1] However, in most cases, pincer complexes are used as homogeneous catalysts, which limits their use in large scale applications due to several factors. Homogeneous catalysts are difficult to recover and reuse, and the isolation and purification of the products are often laborious.

Metallodendrimers are a promising way to support homogeneous catalysts.[2] This approach has several advantages over using traditional homogeneous catalysts. For example, metallodendrimers are soluble in many organic solvents, have well-defined and regular structures, and can be easily recovered by filtration due to their nanometric size. These features make them attractive for designing catalysts, as they allow for the recovery and purification of catalytic products. Therefore, various efforts have been made to develop procedures for the synthesis of pincer-dendrimers.

One of the most common strategies to functionalize a pincer complex is to introduce an easily functionalizing group or anchoring group, such as –OH, $–NH_2$, halogen, alkyne, *etc.*, into the pincer backbone.[3] This approach was pioneered by van Koten and co-workers who reported the reaction of a *para*-hydroxy pincer complex with a dendrimer precursor derived from acyl chlorides (Scheme 1a),[4] while Veggel and Reinhoudt described the synthesis of metallodendrimers of zero order (G_0) by reacting a multi-pincer ligand precursor with a metal source (Scheme 1b).[5] However, both methods were limited to the generation of homometallic species. Despite this limitation, both methodologies were easily carried out in the laboratory.

[a]*Instituto de Química, Universidad Nacional Autónoma de México, Circuito Exterior, Ciudad de México, CP 04510, Mexico. E-mail: damor@unam.mx*
[b]*Centro Conjunto de Investigación en Química Sustentable UAEM-UNAM, Universidad Autónoma del Estado de México, Carretera Toluca-Atlacomulco Km 14.5, Toluca, Estado de México, CP 50200, Mexico. E-mail: qmargarcia@gmail.com*
[c]*Departamento de Química Orgánica y Química Inorgánica, Universidad de Alcalá, Alcalá de Henares 28805, Madrid, Spain*

†Electronic supplementary information (ESI) available. CCDC 2078439–2078442. For ESI and crystallographic data in CIF or other electronic format see DOI: https://doi.org/10.1039/d4dt02841d

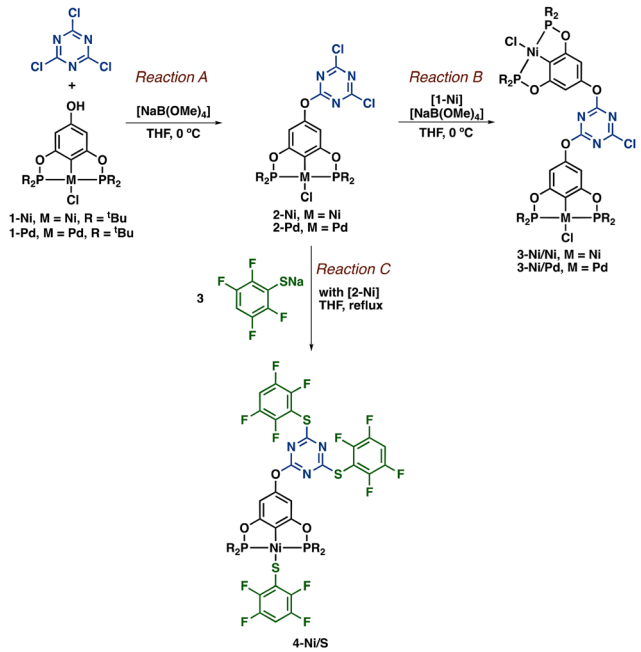

Scheme 1 Synthesis of multimetallic complexes.

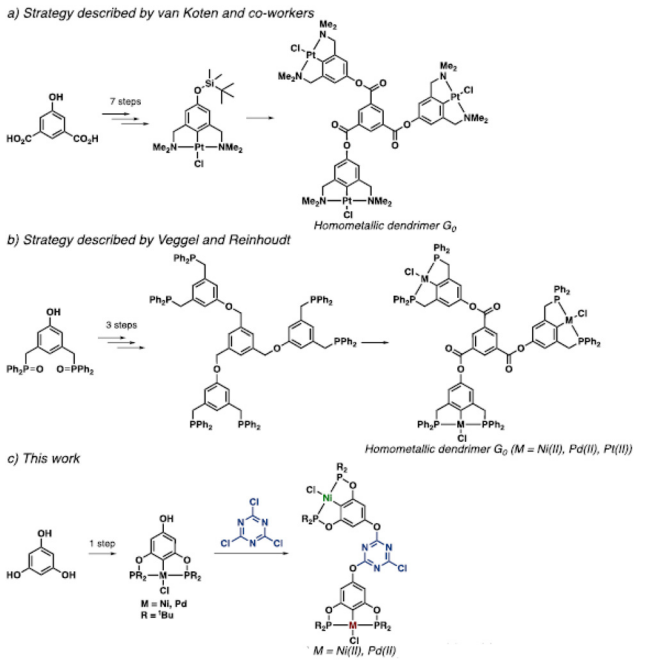

Fig. 1 Reported strategies to obtain pincer-based metallodendrimers.

In our previous work, we successfully synthesized a series of *para*-hydroxy POCOP-pincer complexes and investigated their reactivity towards acyl chlorides to form ester derivatives.[6] Based on these results, we hypothesized that by using these *para*-hydroxy pincers and cyanuric chloride as building blocks, we could control the generation of dendrimers G_0, which would enable the incorporation of different pincer complexes, and ultimately allow for the synthesis of heterometallic species (Scheme 1c). The ability to synthesize heterometallic species has garnered significant attention due to their exceptional catalytic properties, particularly their capacity to perform tandem processes.[7] The incorporation of different pincer complexes into these heterometallic species would also allow for fine-tuning of their catalytic properties for specific applications (Fig. 1).

Results and discussion

To conduct our investigation, we initially carried out the 1 : 1 stoichiometric reaction of a *para*-hydroxy POCOP pincer complex with cyanuric chloride in the presence of $[NaB(OMe)_4]$ at 0 °C, as depicted in Reaction A in Scheme 1. We were able to isolate the functionalized pincer complexes **2-Ni** and **2-Pd** in yields of 80% and 47%, respectively, after workup. The ^{1}H NMR spectra of both complexes showed the absence of the –OH signal, while the ^{13}C NMR spectra exhibited the corresponding signals of the cyanuric chloride at 171 and 173 ppm, respectively. The mass spectra provided us with additional structural information, revealing the molecular ion $[M]^+$ at 655 and 703 *m*/*z*, respectively, confirming the mono-metallic nature of **2-Ni** and **2-Pd**.

With this information, we then explored the reactivity of **2-Ni** and **2-Pd** towards another equivalent of pincer complex **1-Ni** using similar reaction conditions, triazine derivative, **1-Ni**, and $[NaB(OMe)_4]$ in THF at 0 °C, as shown in Reaction B in Scheme 1. We obtained the dimetallic species **3-Ni/Ni** and **3-Ni/Pd** in 53% and 69% yield, respectively. The ^{1}H, ^{13}C, and ^{31}P NMR spectra of complex **3-Ni/Ni** showed a highly symmetrical molecule, whereas complex **3-Ni/Pd** exhibited the presence of two different pincer fragments. The ^{1}H NMR spectrum showed the aromatic proton of the pincer backbone at 6.21 ppm for the Ni fragment and at 6.37 ppm for the Pd moiety. In the ^{31}P NMR spectrum, two signals were observed at 195.1 and 190.4 ppm for the Pd- and Ni-pincer fragment, respectively. Furthermore, the mass spectra of complexes **3-Ni/Ni** and **3-Ni/Pd** showed the molecular ion [M]+ at 1125 and 1173 *m*/*z*, respectively, confirming the proposed structures.

Additionally, we investigated the reactivity of the triazine pincer (**2-Ni**) towards a fluorinated-thiolate (Reaction C, Scheme 1). The high affinity of the thiolate for the metal center led to a ligand exchange, with the chlorine being replaced by the thiolate ligand. The substitution of the chlorine atoms at the triazine moiety by the fluorinated-thiolate also occurred, resulting in the formation of complex **4-Ni/S** in 48% yield. The ^{1}H NMR spectrum of **4-Ni/S** showed the signal of the pincer ligand backbone at 1.34 and 6.18 ppm, while the corresponding signals of the fluorinated-thiolate were observed at 6.60 and 7.10 ppm. The signals of the fluorinated-thiolate in the ^{13}C NMR spectra appeared as multiplets with low intensity due to the ^{19}F–^{13}C coupling. The ^{31}P NMR spectrum displayed only one signal at 190.0 ppm, consistent with the proposed structure. The mass spectrum of **4-Ni/S** showed

the molecular ion $[M]^+$ at 1091 *m*/*z*, confirming the successful synthesis of the complex.

To determine the molecular structures of the complexes, we conducted single-crystal X-ray diffraction analyses. We obtained suitable crystals by slow evaporation of a solution of each complex in a 1 : 1 ethyl acetate/hexane mixture. The crystal data and refinement parameters for each complex are presented in ESI.† Complexes **2-Ni** and **2-Pd** are isostructural and crystallized in a monoclinic system with a space group of $P2_1/n$, while complexes **2-Ni/Pd** and **4-Ni/S** crystallized in a triclinic system with a $P\bar{1}$ space group. The X-ray diffraction analyses allowed us to confirm the proposed molecular structures of each complex.

The molecular structures of complexes **2-Ni**, **2-Pd**, **3-Ni/Pd**, and **4-Ni/S** are shown in Fig. 2. Consistent with our expectations, the metal centers in all complexes are tetracoordinated to two phosphine ligands, one carbon ligand, and one anionic ligand (chlorine or sulfur) and adopt a distorted square-planar geometry. The most significant angles and bond lengths are presented in Table S5 (see ESI†). Notably, the lengths of the Ni–P, Ni–Cl, and Ni–C bonds in all complexes were similar, ranging from 2.18 to 2.24 Å, 2.18 to 2.26 Å, and 1.88 to 1.93 Å, respectively. In contrast, the distances in the Pd pincer fragments were slightly higher, ranging from 2.24 to 2.27 Å, 2.30 Å, and 1.97 to 2.00 Å, respectively. Finally, the Ni–S bond distance was 2.23 Å. All of these measurements were consistent with previous reports.[6,8]

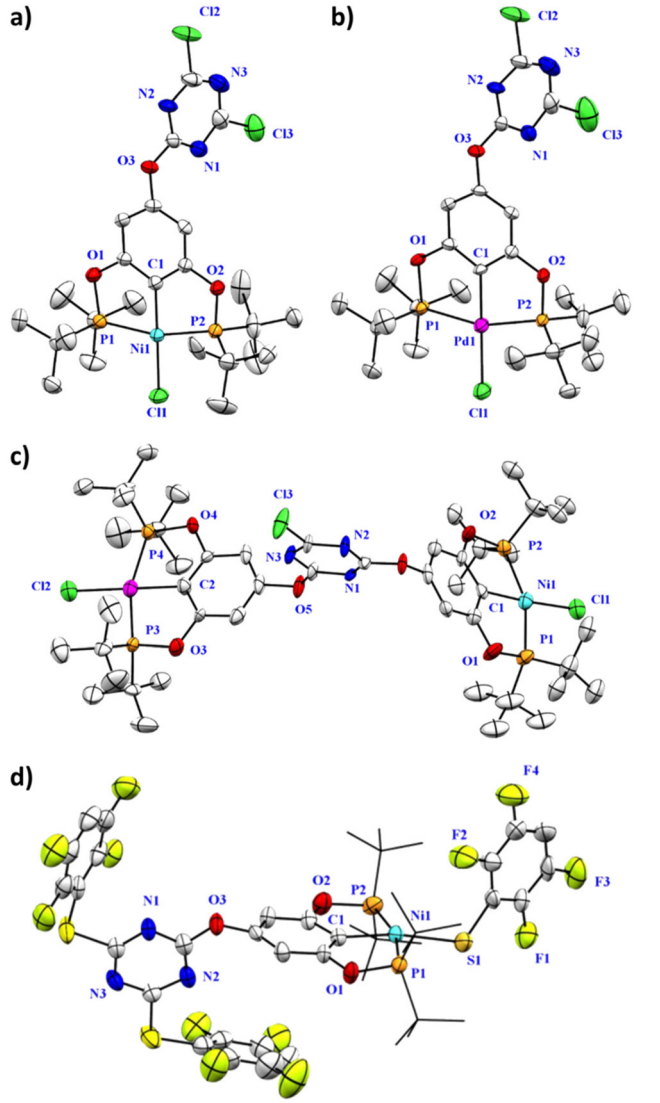

Fig. 2 Molecular structures of (a) **2-Ni**, (b) **2-Pd**, (c) **3-Ni/Pd** and (d) **4-Ni/S**. Hydrogen atoms and disordered counter parts were omitted for clarity. The ellipsoids are represented at 40% probability.

A more detailed study of the X-ray molecular structures revealed that the crystal packing is mainly stabilized by various interactions such as C–H···X (X = N, Cl, and F), π···π and C–F···F (Fig. 3). These interactions play a crucial role in the linkage and stability of the crystal lattice, giving rise to unique topologies in each structure. For example, while **2-Ni** and **2-Pd** complexes have similar molecular structures, their crystal packings are different. Compound **2-Ni** forms monomeric chains in a 1D arrangement along the *c*-axis through C–H···Cl–Ni intermolecular interactions between neighboring molecules with a H···Cl distance of around 2.87 Å (Fig. 3a). In contrast, **2-Pd** shows two C–H···Cl–Pd intermolecular interactions, one between the hydrogen of the phenyl moiety and Cl(1)–Pd(1), and the other between the *tert*-butyl moiety and Cl(1)–Pd(1), with a distance of 2.83 Å for both cases. Additionally, a π···π intermolecular interaction was observed through the (C_3N_3) aromatic rings of (C_3N_3) triazine fragments, which are found almost eclipsed *face-to-face* in an antiparallel disposition with a distance between centroid–centroid of 3.68 Å (Fig. 3b). This results in the formation of a symmetric dimeric species and a 2D arrangement in the direction of the *bc*-axes (Fig. 3b).

Compound **3-Ni/Pd** also exhibits a dimeric structure that is generated by two intermolecular hydrogen bonds and a π···π interaction (Fig. 3c). The two C–H···N hydrogen bonds are formed between the hydrogen H4 of the phenyl moiety and a nitrogen atom of the triazine fragment, with a distance of 2.54 Å. In addition, a π···π interaction is observed between the (C_3N_3) triazine fragments, which are almost eclipsed *face-to-face* in an antiparallel π-stacking, with a distance between the centroids of 3.81 Å. These dimeric species form columns that run along the *a*-axis.

Compound **4-Ni/S** is stabilized primarily by intermolecular interactions such as C–H···F–C, C–H···S–C, and C–F···F–C (Fig. 3d, e and S21†). The F···F non-bonded distances are found in the range of 2.86–2.93 Å with angles ranging from 107–110° (Fig. 3d), and these distances are slightly shorter than the sum of van der Waals radii ($F\cdots F_{rvdw}$ = 2.94 Å). The pincer molecules are linked by intermolecular C–H···S–C hydrogen bonds with an H···S distance of 2.90 Å, resulting in a 1D chain structure along the *c*-axis (Fig. S21†). The fluorinated thiol fragments also participate in C–F···F–C interactions, which help to stabilize the 1D arrangement. Additionally, C–H···F and C–H···N (Fig. S22†) hydrogen bonds were observed with distances of 2.53 and 2.72 Å, respectively.

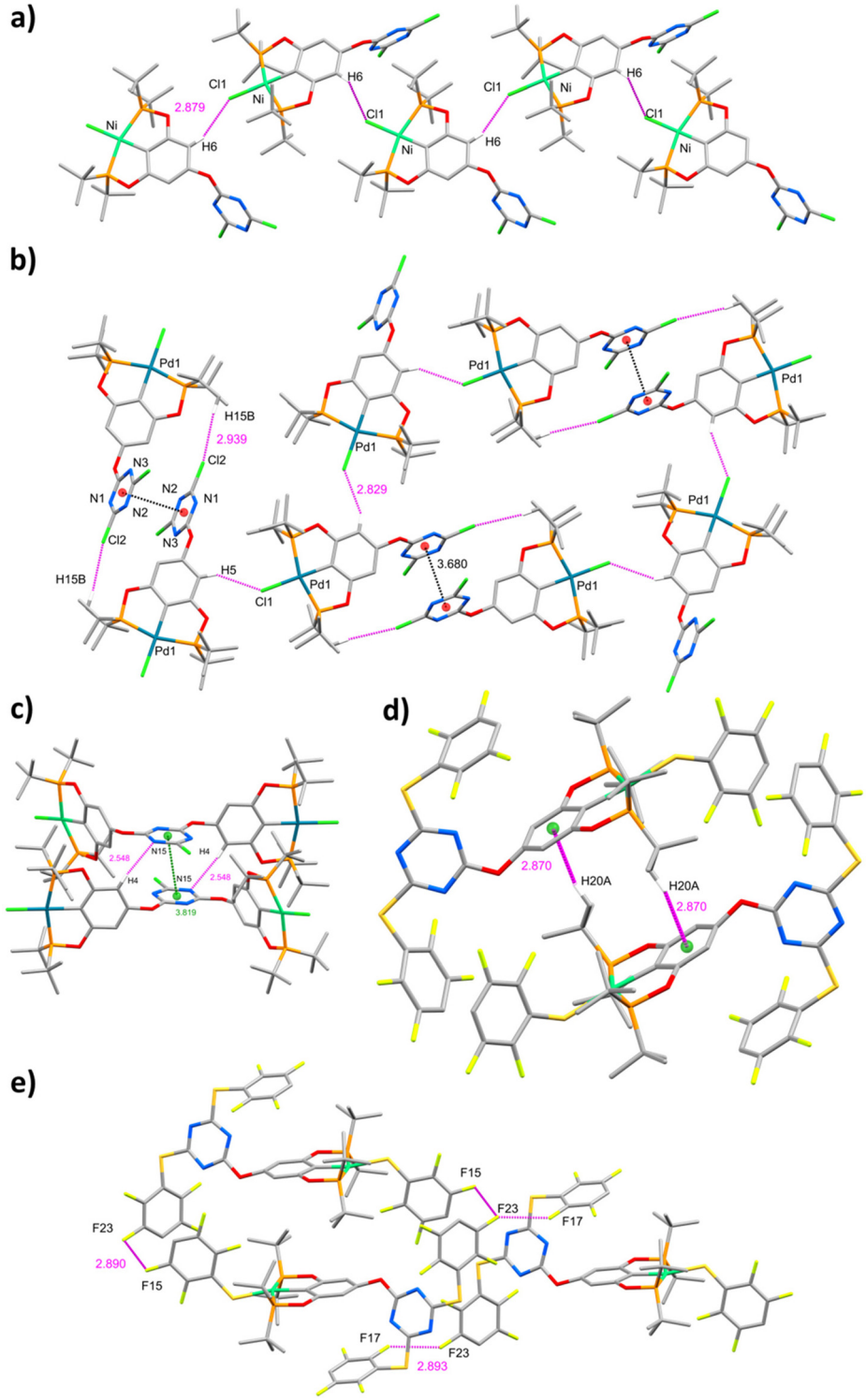

Fig. 3 (a) C–H···Cl interactions observed in compound **2-Ni**. (b) C–H···Cl and π···π interactions observed in compound **2-Pd**. (c) C–H···N and π···π interactions observed in **3-Ni/Pd**. (d) C–H···π and C–F···F interactions observed in compound **4-Ni/S** (e) 1D chain formed by C–F···S hydrogen bonds in **4-Ni/S**.

We employed the CrystalExplorer program[9] to generate Hirshfeld surfaces for **2-Ni**, **2-Pd**, **3-Ni/Pd**, and **4-Ni/S**. In Fig. S23,† the Hirshfeld surface of all complexes is depicted, highlighting regions of close contact (red dots) analyzed *via* the d_{norm} function. Complexes **2-Ni** and **2-Pd** exhibited similar crystalline packaging, with similar d_{norm} and shape-index func-

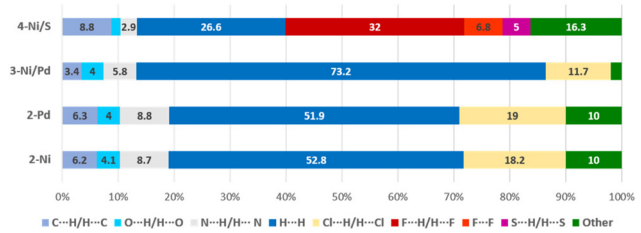

Chart 1 Plot of percentages of contacts observed in compounds **2-Ni**, **2-Pd**, **3-Ni/Pd** and **4-Ni/S**.

tion maps (Fig. S23a–S23d†). Analysis of compound **3-Ni/Pd** confirmed the presence of CH···N and π···π interactions (Fig. S23e and S23f†). Additionally, the d_{norm} mapping for **4-Ni/S** indicated strong hydrogen bond interactions (Fig. S23g†), particularly the C–H···C hydrogen bond between a C–H of the pincer ring and the fluorinated ring.

Furthermore, fingerprints of the Hirshfeld surfaces were obtained for **2-Ni**, **2-Pd**, **3-Ni/Pd**, and **4-Ni/S** (Table S7†). Despite having different metal centers, compounds **2-Ni** and **2-Pd** displayed similar percentage contributions due to the maintenance of similar contact types. The most significant contributions were attributed to N···H/H···N and Cl···H/H···Cl interactions, depicted as symmetrical points across the diagonal in Table S7.† Similarly, compounds **3-Ni/Pd** and **4-Ni/S** displayed comparable patterns. However, in **4-Ni/S**, the absence of chlorine atoms precluded Cl···H/H···Cl interactions, replaced instead by F···H/H···F contacts, observed at a higher percentage due to the increased number of fluorine atoms. Additionally, compound **4-Ni/S** exhibited fluorine F···F (6.3%) and S···H/H···S (5.0%) contacts (Chart 1).

Conclusions

In summary, the solid-state structures of the complexes **2-Ni**, **2-Pd**, **3-Ni/Pd**, and **4-Ni/S** were investigated using single-crystal X-ray diffraction. The molecular structures indicate that the Ni (II) and Pd(II) centers exhibit a distorted square-planar environment and the POCOP pincer ligand coordinates to the metallic atom in a typical meridional fashion. Complexes **2-Ni** and **3-Ni/Pd** are monomeric structures, whereas the complexes **2-Ni** and **3-Ni/Pd** adopt a dimeric structure. In the crystal lattice, complexes **2-Ni** and **4-Ni/S** exhibit a 1D arrangement through C–H···X (X = Cl, S), while the **3-Ni/Pd** complex displays a 2D arrangement due to C–H···Cl and π···π interactions. The crystal packing of **4-Ni/S** is particularly intriguing due to the presence of C–F···F and C–F···H interactions. The interactions were supported by the determinations of Hirshfeld surface plots. Overall, these findings provide insights into the structural properties of these complexes and may facilitate the design and synthesis of novel materials with desirable properties.

The presented methodology for the functionalization of *para*-hydroxy pincer complexes offers a straightforward approach for the synthesis of multimetallic species. Also, this methodology has the potential to be extended to other pincer complexes, opening up the possibility of creating a diverse range of dendritic architectures with various functional groups. These dendritic architectures could have a broad range of applications beyond catalysis, including drug delivery, sensors, and molecular recognition. The simplicity and efficiency of the methodology make it an attractive option for the scalable synthesis of these complex materials. Thus, we believe that this methodology will have a significant impact on the fields of materials science and catalysis, and it holds promise for the development of new and innovative technologies.

Author contributions

J. S. S.-G and M. A. G.-E. performed the experiments. A. A.-C. and E. R.-F. performed the supramolecular analyses. All authors were involved in the conceptual design of the study, discussed the results and wrote the manuscript.

Data availability

The data supporting this article has been included as part of the ESI.†

Conflicts of interest

There are no conflicts to declare.

Acknowledgements

E. R. F. would like to thank Programa de Becas Posdoctorales-DGAPA-UNAM for postdoctoral scholarships (Oficio: CJIC/CTIC/1139/2020). A. A.-C. is grateful to CONAHCyT for the postdoctoral fellowship (Estancias posdoctorales por México 2022(1)). H. V. would like to thank the Generalitat de Catalunya for a Beatriu de Pinós contract (2019-BP-0080). D. M-M gratefully acknowledges CONAHCYT (A1-S-033933) and DGAPA-UNAM (PAPIIT IN223323) for generous financial support. And Dr. Ruben A. Toscano for its helpful support on the crystallographic part.

References

1 (*a*) H. Valdés, E. Rufino-Felipe, G. van Koten and D. Morales-Morales, *Eur. J. Inorg. Chem.*, 2020, **2020**, 4418; (*b*) H. Valdés, M. A. García-Eleno, D. Canseco-Gonzalez and D. Morales-Morales, *ChemCatChem*, 2018, **10**, 3136; (*c*) H. Valdes, J. M. German-Acacio, G. van Koten and D. Morales-Morales, *Dalton Trans.*, 2022, **51**, 1724; (*d*) L. Alig, M. Fritz and S. Schneider, *Chem. Rev.*, 2019, **119**, 2681; (*e*) A. Mukherjee and D. Milstein, *ACS Catal.*, 2018, **8**,

11435; (*f*) *Pincer Compounds Chemistry and Applications*, ed. D. Morales-Morales, Elsevier, 2018; (*g*) A. Kumar, T. M. Bhatti and A. S. Goldman, *Chem. Rev.*, 2017, **117**, 12357; (*h*) M. Asay and D. Morales-Morales, *Dalton Trans.*, 2015, **44**, 17432; (*i*) M. Asay and D. Morales-Morales, *Top. Organomet. Chem.*, 2016, **54**, 239; (*j*) C. Gunanathan and D. Milstein, *Chem. Rev.*, 2014, **114**, 12024; (*k*) K. J. Szabó and O. F. Wendt, *Pincer and Pincer–Type Complexes: Applications in Organic Synthesis and Catalysis*, Wiley-VHC, 2014; (*l*) K. J. Szabó, *Top. Organomet. Chem.*, 2013, **40**, 203; (*m*) G. van Koten, in *Organometallic Pincer Chemistry*, ed. G. van Koten and D. Milstein, Springer Berlin Heidelberg, Berlin, Heidelberg, 2013, p. 1; (*n*) N. Selander and K. J. Szabó, *Chem. Rev.*, 2011, **111**, 2048; (*o*) J. Choi, A. H. R. MacArthur, M. Brookhart and A. S. Goldman, *Chem. Rev.*, 2011, **111**, 1761; (*p*) D. Morales-Morales, *Rev. Soc. Quim. Mex.*, 2004, **48**, 338; (*q*) M. E. Van Der Boom and D. Milstein, *Chem. Rev.*, 2003, **103**, 1759; (*r*) M. Albrecht and G. Van Koten, *Angew. Chem., Int. Ed.*, 2001, **40**, 3750.

2 (*a*) N. J. M. Pijnenburg, T. J. Korstanje, G. van Koten and R. J. M. K. Gebbink, in *Palladacycles*, 2008, pp. 361; (*b*) R. A. Gossage, L. A. van de Kuil and G. van Koten, *Acc. Chem. Res.*, 1998, **31**, 423; (*c*) H. P. Dijkstra, N. Ronde, G. P. M. van Klink, D. Vogt and G. van Koten, *Adv. Synth. Catal.*, 2003, **345**, 364; (*d*) H. P. Dijkstra, M. Albrecht, S. Medici, G. P. M. van Klink and G. van Koten, *Adv. Synth. Catal.*, 2002, **344**, 1135; (*e*) A. W. Kleij, R. A. Gossage, R. J. M. Klein Gebbink, N. Brinkmann, E. J. Reijerse, U. Kragl, M. Lutz, A. L. Spek and G. van Koten, *J. Am. Chem. Soc.*, 2000, **122**, 12112; (*f*) A. W. Kleij, R. A. Gossage, J. T. B. H. Jastrzebski, J. Boersma and G. van Koten, *Angew. Chem., Int. Ed.*, 2000, **39**, 176; (*g*) C. Schlenk, A. W. Kleij, H. Frey and G. van Koten, *Angew. Chem., Int. Ed.*, 2000, **39**, 3445.

3 (*a*) H. Valdés, L. González-Sebastián and D. Morales-Morales, *J. Organomet. Chem.*, 2017, **845**, 229; (*b*) H. Valdés, J. M. Germán-Acacio and D. Morales-Morales, in *Organic Materials as Smart Nanocarriers for Drug Delivery*, ed. A. M. Grumezescu, Elsevier – William Andrew, 2018, pp. 245; (*c*) M. Q. Slagt, D. A. P. V. Zwieten, A. J. C. M. Moerkerk, R. J. M. K. Gebbink and G. V. Koten, *Coord. Chem. Rev.*, 2004, **248**, 2275.

4 P. J. Davies, D. M. Grove and G. van Koten, *Organometallics*, 1997, **16**, 800.

5 W. T. S. Huck, B. Snellink-Ruël, F. C. J. M. van Veggel and D. N. Reinhoudt, *Organometallics*, 1997, **16**, 4287.

6 (*a*) M. A. García-Eleno, E. Padilla-Mata, F. Estudiante-Negrete, F. Pichal-Cerda, S. Hernández-Ortega, R. A. Toscano and D. Morales-Morales, *New J. Chem.*, 2015, **39**, 3361; (*b*) M. K. Salomón-Flores, I. J. Bazany-Rodríguez, D. Martínez-Otero, M. A. García-Eleno, J. J. Guerra-García, D. Morales-Morales and A. Dorazco-González, *Dalton Trans.*, 2017, **46**, 4950.

7 (*a*) J. A. Mata, F. E. Hahn and E. Peris, *Chem. Sci.*, 2014, **5**, 1723; (*b*) S. Patra and N. Maity, *Coord. Chem. Rev.*, 2021, **434**, 213803; (*c*) R. Clauss, S. Baweja, D. Gelman and E. Hey-Hawkins, *Dalton Trans.*, 2022, **51**, 1344; (*d*) Z. Wen, E. Maisonhaute, Y. Zhang, S. Roland and M. Sollogoub, *Chem. Commun.*, 2022, **58**, 4516; (*e*) Y. Li, C. Wang, Q. Chen, H. Li, Y. Su, T. Cheng, G. Liu and C. Tan, *Chem. – Asian J.*, 2021, **16**, 2338.

8 (*a*) E. G. Morales-Espinoza, R. Coronel-García, H. Valdés, R. Reyes-Martínez, J. M. German-Acacio, B. A. Aguilar-Castillo, R. A. Toscano, N. Ortiz-Pastrana and D. Morales-Morales, *J. Organomet. Chem.*, 2018, **867**, 155; (*b*) M. Joksch, A. Spannenberg and T. Beweries, *Acta Crystallogr., Sect. E: Crystallogr. Commun.*, 2019, **75**, 1011; (*c*) M. Joksch, H. Agarwala, J. Haak, A. Spannenberg and T. Beweries, *Polyhedron*, 2018, **143**, 118; (*d*) M. Joksch, J. Haak, A. Spannenberg and T. Beweries, *Eur. J. Inorg. Chem.*, 2017, **2017**, 3815; (*e*) M. A. Garcia-Eleno, M. Quezada-Miriel, R. Reyes-Martinez, S. Hernandez-Ortega and D. Morales-Morales, *Acta Crystallogr., Sect. C: Struct. Chem.*, 2016, **72**, 393; (*f*) S. Lapointe and D. Zargarian, *Dalton Trans.*, 2016, **45**, 15800; (*g*) V. Pandarus and D. Zargarian, *Organometallics*, 2007, **26**, 4321.

9 P. R. Spackman, M. J. Turner, J. J. McKinnon, S. K. Wolff, D. J. Grimwood, D. Jayatilaka and M. A. Spackman, *J. Appl. Crystallogr.*, 2021, **54**, 1006.